Epitaxial Issues and Growth Morphologies of InAlAs/InGaAs
MQWs and Heterostructures on (100) and non -(100) InP Substrates

by

Aris Christou
Materials Science and Engineering
University of Maryland, College Park, MD 20742 USA and

Abstract

InP Substrate orientation (100)A, (100)B, (110)A, (110)B, (111)A, (111)B, (112)A and (112)B can control the kinetics of growth and also significantly affects phase decomposition and ordering. Through TEM, and AFM investigations, the interfacial and surface morthologies of layers grown on the above surfaces has been determined. Features related to phase decomposition due to (110)A, (111)B and (112)B surfaces have been identified. Anisotropy in optical transitions in samples grown on (110)A and (110)B InP has been identified through photoreflectance investigations. Surface roughness is directly due to the substrate orientation and not due to the growth parameters.

1. Introduction

Traditional InP based semiconductor compounds have been grown by molecular beam and chemical vapor deposition techniques of (100) oriented substrates, resulting in smooth epitaxial surfaces. On the other hand, pseudomorphic growth of III-V heterostructures on non-(001) InP substrates have been investigated comprehensively since 1994 as shown by the initial publications [1-4] reporting phase decomposition and growth related defects including anti-phase domains. We may summarize these results for the (110), (111) and (112) InP substrates as follows:

(110) InP results in a polarization anisotropy [1,2,5,6],

(111) InP shows a strong piezoelectric effect along the growth direction [7], and

(112) InP also shows a strong polarization anisotropy for modulators and polarizers [8].

Reported polarization control of vertical channel surface emitting lasers (VCSELs) through use of an anisotropic gain distribution in (110) oriented strained quantum well structures has indicated the renewed importance of non (100) substrates for optics applications [9,10]. Anisotropy in the gain distribution was observed for the first time as well as second-order nonlinear polarization and harmonic generation in (112) InP based VCSELs.

A comprehensive investigation on the epitaxial growth by MBE of InAlAs on InGaAs on InP Substrates oriented as – (100), (110)A, (110)B, (111)A, (111)B, (112)A, (112)B, is reported. The objective of these investigations was to determine the influence of substrate orientation on possible alloy decomposition and ordering. Table 1 shows the double layer structure on InP. For comparison, we also grew a series of InAlAs with Al mole fraction of 0.478. Table 2 shows a comprehensive list of samples grown as a function of growth temperature and arsenic pressure. The experiments were so designed as to show the substrate effect as the degree of tilt away from

the traditional (100) orientation increases, hence we were able to also investigate the (112) orientation and compare it with both the (110) and the (111).

Specimen analysis on all samples were carried out using transmission electron microscopy, either as plane view microscopy denoted as (PVTEM) or as cross-sectional microscopy denoted as (XTEM). Additionally, high resolution transmission electron microscopy (HRTEM) was utilized to identify ordering whenever necessary. Atomic force microscopy (AFM) was also applied in order to identify and measure surface roughness on all samples. Through correlation of these techniques we now have a clear understanding of the reasons for surface roughness and for the origin of interfacial defects.

2. Experimental Results

The results of the present comparitive investigation show that growth on (100) and (110)B index substrates resulted in smooth surfaces, without roughness, and hence without growth generated defects. However, growth on (110)A InP substrates resulted in pronounced roughness oriented along the $[\bar{2}20]$. These observations of surface roughness are general in nature and were detected on all samples grown on (110)B substrates shown in Table 2. They are not affected by arsenic over-pressure indicating that the growth conditions on non - (100) InP were optimal. Growth temperature also did not affect surface morphology but probably only affected factors related to surface diffusion. From AFM, the distance between hillocks was determined to be 90-95 nm. In addition, using XTEM techniques, we observed contrast stripes in the InAlAs inclined 8-12 degrees with respect to the horizontal. These contrast stripes are due to anti-phase domain boundaries (APBs) that separate the ordered micro-domains that exist in these layers. These APBs create the surface roughness when they propagate to the sample

surface. We concluded that sample roughness was related to contrast inhomogeneities due to composition modulation as reported by Guyer (9). The transmission electron diffraction (TED) patterns show two diffuse intensity maximum between 220 and 440 indicating CuAu I-type ordering on (110) planes. From such TED analysis we confirmed that the contrast stripes were APBs breaking the ordered microdomains. The presence of two maxima dividing the (220) vector in three equal pieces indicates that the ordered structures have a periodicity of three atomic planes, with every third plane being aluminum atoms. Neither stacking faults nor threading defects are observed in these samples.

On the other hand, growth on (111)B InP resulted in a high density of inverted pyramid defects and a faint roughness in the $[20\bar{2}]$ direction. The growth on (112)B InP showed a high density of the same crater defects (inverted triangular faceted pyramid). Lateral phase decomposition was also evident. The comparison of the above samples indicates no dependence on the mole fraction of aluminum. Table 4 summarizes the defects present on InAlAs surfaces grown on both (111)B and (112)B. These pyramid structures present faceted faces, forming inverted pyramids (Fig.1). The XTEM analysis allowed us to approximate the orientation of each facet. From other XTEM images, it is apparent that these inverted pyramids originated at the InGaAs/InP interface, and grew to the sample surface crossing both (InGaAs and InAlAs) layers. The origin of these faceted defects was due to the growth inhibition of the InGaAs layer over the InP substrate. These samples also presented an important lateral contrast modulation, which was deduced from the XTEM observation. This contrast modulation was also initiated at the InGaAs/InP interface and then extended to the remainder of the layer, continuing to the InAlAs upper layer. The lateral contrast modulation can be due to lateral decomposition or to a pure

strain contrast. There is slight evidence of an ordered structure of CuPt-type. Due to the weakness of diffraction pattern maxima one cannot entirely conclude that the contrast is due to ordering. The XTEM data shows a quasi-periodic structure of contrast stripes perpendicular to growth axis of the InAlAs and InGaAs layers. These images are summarized by the schematic of Fig. 1.

Samples on (112)B InP substrate: In general, these surfaces are covered by faceted crater defects with inverted pyramid shape (Fig. 1). These defects are formed in the InGaAs layer which was initially grown on the InP substrate. The presence of the defects does not depend on arsenic pressure, nor on growth temperature.

The smooth surfaces, characteristic of the layers grown on (110)B is shown in the AFM images of Fig. 2. The morphology of Fig. 2 is characteristic of all samples grown on (110)B and does not depend on aluminum mole fraction or growth temperature. In addition, arsenic overpressure, does not appear to be the primary reason for smooth surface formation. Typical surface roughness indicating periodic hillocks on (110)A surfaces is shown in Fig. 3. Such hillock formation extended over the entire lateral surface, and probably originated from the roughness of the APBs shown in Fig. 3. The TEM images show the inclined APBs in the InAlAs layer and the lateral APBs in the InGaAs layer (Fig. 4). The TED patterns of Fig. 5 again confirmed the type of order present in the heterostructures grown on (110)A InP. In contrast to (110)A and (110)B InP, the structures grown on (111)B and (112)B InP resulted in a different morphology. Fig. 6 shows typical triangular pyramid defects on heterostructures grown on (112)B InP. The origin of the triangular defects is the surface of the InP substrate at locations of

local compositional perturbations or surface steps of undetermined origin. InAlAs grown on (111)A and (112)A did not show the presence of triangular defects and hence the B orientation is critical to the formation of such defects. The smooth surfaces on “B” type (110) substrates are presented first in the AFM images which follow. These surfaces were observed on all (110)B samples and were independent of arsenic pressure and growth temperature.

Two diffuse diffraction spots between the 220 and 440 reflections for (110)A is shown in Fig. 5. The division of the 220 vector into three parts indicates that every third atomic plane is a mono-atomic platelet. This also indicates that the distance between the matrix and the diffuse spots is slightly larger than (1/3) g_{220}. In direct space, this corresponds to a smaller interplanar (110) distance between the platelets. Since aluminum atoms have a smaller radius than In or Ga, then every third plane is occupied by aluminum atoms. The contrast modulation must then be due to compositional modulation because of the presence of aluminum in the InAlAs compound. The compound InAlAs is therefore more susceptible to contrast modulation than the InGaAs compound.

Fig. 6 shows the faceted craters for growth on (112)B InP which were similar to growths on (111)B InP. The facet formation may be explained by the different growth velocities on the inclined planes. Growth inhibition therefore created these faceted structures, and their extent does depend on surface diffusivity differences.

3. Conclusions

We have reported the effect of the InP substrate orientation on the surface morphology of InAlAs deposited by molecular beam epitaxy on InGaAs buffer layers. The phosphorus termination of the InP substrate and the defects generated at the buffer layer – substrate interface, rather than the growth parameters, determines the surface morphology of InAlAs grown on non – (100) InP. These defects ranged from anti-phase domain boundaries (APBs) to triangular pyramid defects to surface hillocks. Surface structure indicative of APB formation and phase decomposition was indicative of InAlAs grown on (110)A InP. Such morphologies were not significantly affected by growth temperature nor arsenic overpressure. In contrast, InAlAs/InGaAs layers grown on (110)B InP substrates were smooth without noticeable unique surface morphologies. It has also been shown by the present investigation that on (110)A substrates regions of InAlAs layers had CuAuI type ordering and composition modulation. These morphologies were caused by the presence of aluminum and hence was weakly affected by the growth temperature. The pyramid faceted craters likewise were observed in InAlAs/InGaAs layers grown on (111)B and (112)B indexed InP substrates. In addition, evidence of lateral contrast modulation was also present. A preliminary investigation of optical anisotropy in InAlAs on non – (100) InP substrates showed evidence of in-plane optical anisotropy on (110)A and (110)B InP substrates. The optical anisotropy was not observed in InAlAs grown on (100) InP.

3. Acknowledgements

The authors thank Prof. Salamanca-Riba for assistance in the analysis of some of the InAlAs/InGaAs/InP samples. The authors acknowledge the assistance of R. Leavitt of the Army Research Laboratory for the MBE growth of some of the samples. The investigations were supported by the ARL-UMD cooperative research agreement in microelectronics.

4. References

1. X. Chen, C. H. Malloy, D. J. Someford, J. Sharma, J. Appl. Phys. Lett. 67, 1393 (1995).
2. Y. Okuno, T. Tsuchiya and M. Okai, Appl. Phys. Lett. 71, 1918 (1997).
3. E. Bhat, M. A. Koza, D. M. Hwang, M. Brasil, R. E. Nahory, J. Crystal Growth 124, 311 (1992).
4. G. J. Rees, J. Microelec. 28, 957 (1997).
5. M. Mitsuhara, M. Okamoto, R. Iga, T. Yamada, J. Crystal Growth 136, 195 (1994).
6. N. D. Zakharov, Z. Liliental-Weber, W. Swider, J. Wasburn, A. S. Brown and R. Metzger, J. Elec. Mat.22, 1495 (1993).
7. J. E. Guyer and P. Voorhees, J. Crystal Growth 187, 150 (1998).
8. J. Mawst, A. Bhattacharya, J. Lopez, D. Botez, D. Z. Garbuzov, L. DeMarco, J. C. Connolly, M. Jansen, F. Fang and R. F. Nabiev, Appl. Phys. Lett. 69, 1532 (1996).
9. N. D. Whitbread and P. N. Robson, IEEE J. Quantum Electron. 30, 139 (1994).
10. J. A. Armstrong, N. Bloembergen, J. Ducuing and P. S. Pershan, Phys. Rev. 127, 1918 (1962).

Materials Grown	X, Mole Fraction
50nm $In_{1-x} Al_x As$	0.478 – 0.518

50 nm $In_{0.53}Ga_{0.47}As$	0.53
InP Substrate Orientation: (100), (110)A, (110)B, (111)A, (111)B, (112)A, (112)B	

Table 1. Layers grown on InP of various orientations, and on one 50 nm $In_{0.53}Ga_{0.47}As$ buffer layer.

Sample No.	Substrate Orientation	Al Mole Friction	Growth Temperature (^oC)	As Pressure, $1x10^{-5}$ Torr
695	(100)A and B	0.478	544 ^oC	1.10
	(110)A, (110)B	0.478	544 ^oC	1.10
	(111)A, (111)B	0.478	544 ^oC	1.10
	(112)A, (112)B	0.478	544 ^oC	1.10
697	(100)	0.518	544 ^oC	1.64
	(110)A, (110)B	0.518	544 ^oC	1.64
	(111)A, (111)B	0.518	544 ^oC	1.64
	(112)A, (112)B	0.518	544 ^oC	1.64
698	(100)	0.518	562^oC	1.64
	(110)A, (110)B	0.518	562^oC	1.64
	(111)A, (111)B	0.518	562^oC	1.64
	(112)A, (112)B	0.518	562^oC	1.64
699	(100)	0.518	544 ^oC	0.65
	(110)A, (110)B	0.518	544 ^oC	0.65
	(111)A, (111)B	0.518	544 ^oC	0.65
	(112)A, (112)B	0.518	544 ^oC	0.65
705	(110)A, (110)B	0.478	567 ^oC	1.73
	(111)A, (111)B	0.478	567 ^oC	1.73
	(112)A, (112)B	0.478	567 ^oC	1.73
706	(110)A, (110)B	0.478	522^oC	1.10
	(111)A, (111)B	0.478	522^oC	1.10
	(112)A, (112)B	0.478	522^oC	1.10

Table 2. Summary of the samples grown for the present investigation. The set of samples 697 and 705 were grown under excess arsenic conditions inorder to compare the degree of surface roughness under these conditions.

Sample No.	Orientation	Al Mole Fraction	Distance Between Hillocks, (nm)

695	(110)A (111)A	0.478 0.478	103 110
697	(110)A (111)A	0.518 0.518	95 102
698	(110)A (111)A	0.518 0.518	91 95
706	(110)A (111)A	0.478 0.478	78 85

Table 3. Hillocks separation distance measured for the series of (110)A and (111)A samples. Growth on (110)A resulted in a shorter separation distance in comparison to growth (111)A surfaces.

Sample No.	Orientation of Substrate	Hillocks Separation Distance(nm)	Density of Oval Defects 10^{7} cm^{-2}
697	(111)B (112)B	142 135	10 10
698	(111)B (112)B	106 100	10 8 - 9
699	(111)B (112)B	72 65	2 7 - 8

Table 4. Comparison of Hillock Separation Distance and Density of Oval Defects for Samples Grown on (111)B and (112)B.

List of Figure Captions

Fig. 1. Schematic of inverted pyramid structures in samples (111)B and (112)B. Letters A, B and C label the three edge projections on sample surface.

Fig. 2a) AFM image of sample 695 (110)B. The surface is completely smooth and lacking any indication of roughness. Similar smoothness was evident on all (110)B surfaces.**Fig. 2b)** 3D AFM image of sample 695 (110)B again indicates smoothness. Similar morphologies were observed for samples 697, 698, 699, 705 and 706.

Fig. 3. AFM image of a typical InAlAs/InGaAs heterostructure grown on the (110)A surface of sample 697. Periodic surface roughness shown is indicative of all samples grown on "A" type surfaces.

Fig. 4. Cross-sectional TEM of InAlAs/InGaAs grown on (110)A showing the inclined APBs. These APBs resulted in a surface roughness consisting of wave like hillocks separated by distances listed in Table 3.

Fig. 5. TED pattern of samples grown on (110)A showing ordering present in the InAlAs layer.

Fig. 6a) PVTEM micrograph of sample 695 (112)B. The triangle faceted defects are homogeneously distributed on the sample surface. **Figure 6b**. Cross-sectional TEM image of sample 695 (112) InP. The triangle defects have a faceted structure.

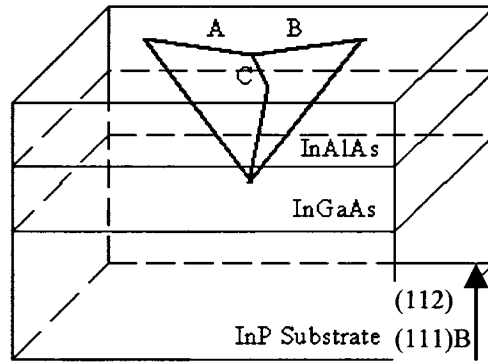

Edges' Projections	(111)B	(112)
A	$11\bar{2}$	$11\bar{1}$
B	$\bar{2}11$	$\bar{3}11$
C	$1\bar{2}1$	$1\bar{3}1$

Fig. 1. Scheme of inverted pyramid structures in samples (111)B and (112)B. Letters A, B and C label the three edge projections on sample surface.

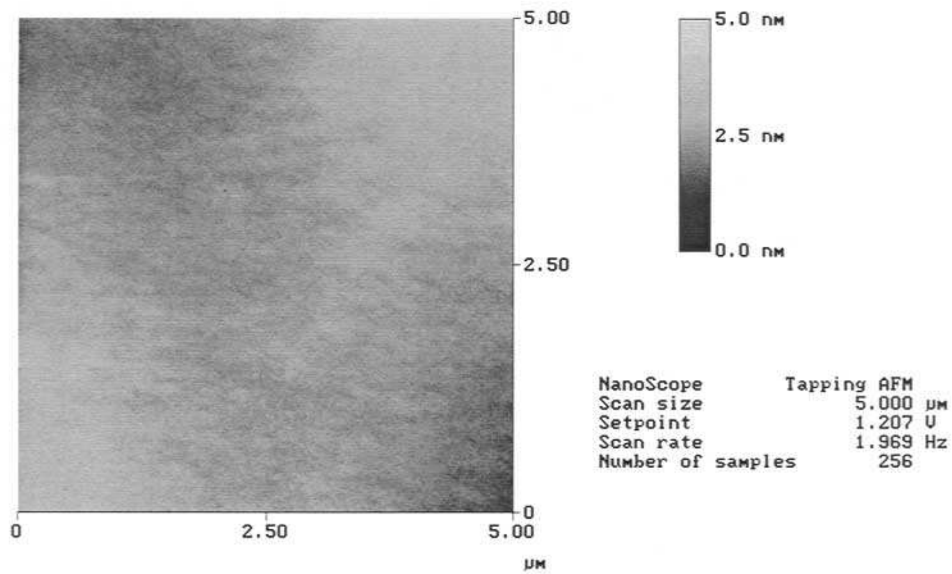

(a)

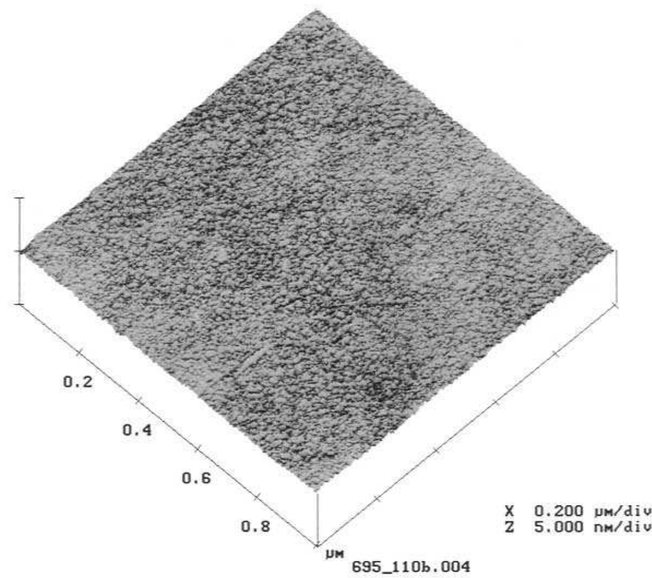

(b)

Fig. 2a) AFM image of sample 695 (110)B. The surface is completely smooth and lacking any indication of roughness. Similar smoothness was evident on all (110)B surfaces.**Fig. 2b)** 3D AFM image of sample 695 (110)B again indicates smoothness. Similar morphologies was observed for samples 697, 698, 699, 705 and 706.

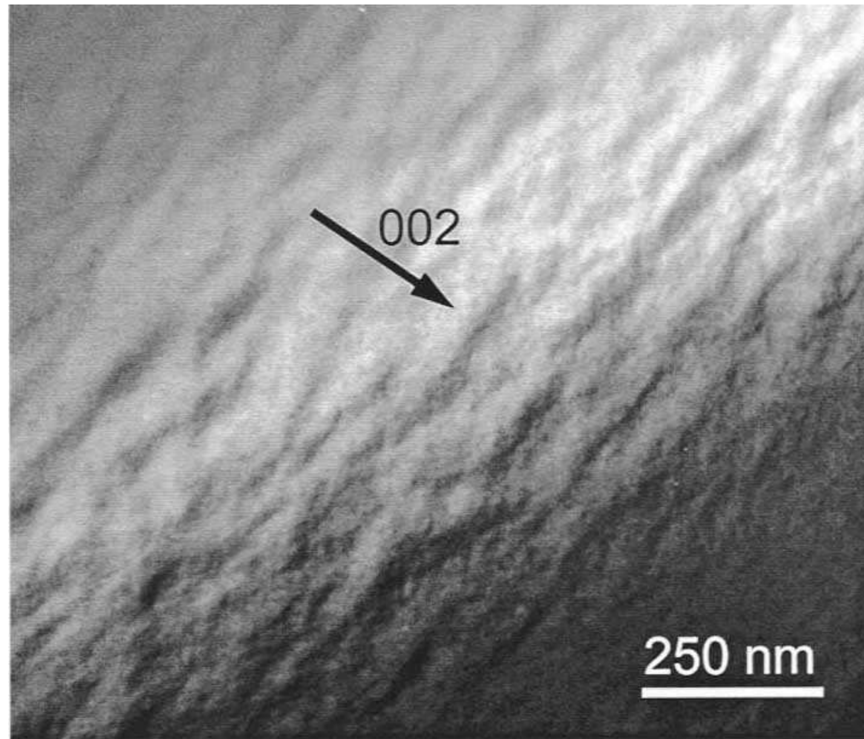

Fig. 3. AFM image of a typical InAlAs/InGaAs heterostructure grown on the (110)A surface of sample 697. Periodic surface roughness shown is indicative of all samples grown on "A" type surfaces.

Fig. 4. Cross-sectional TEM of InAlAs/InGaAs grown on (110)A showing the inclined APBs. These APBs resulted in a surface roughness consisting of wave like hillocks separated by distances listed in Table 3.

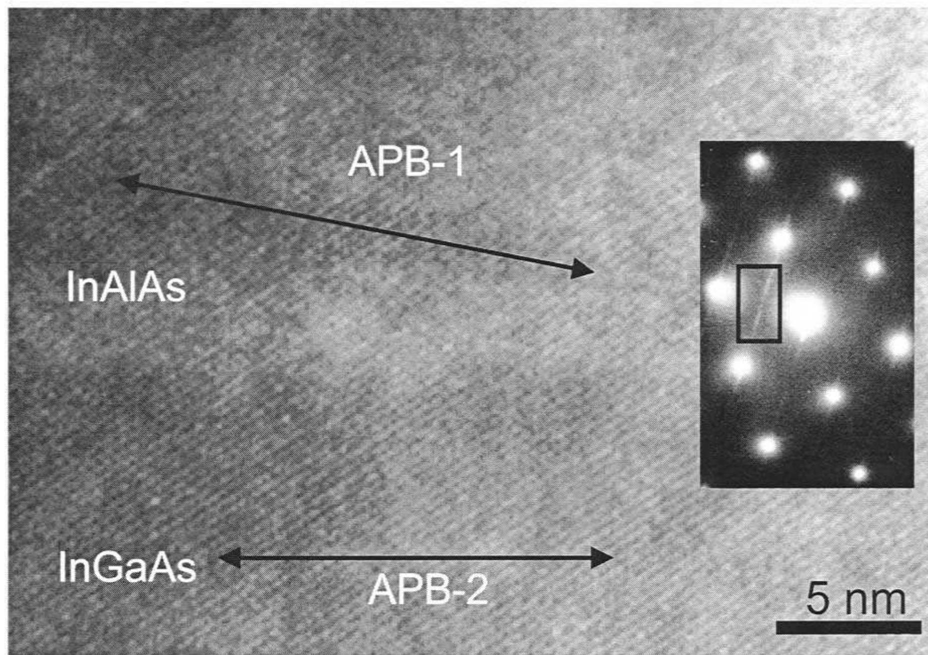

Fig. 5. TED pattern of samples grown on (110)A showing ordering present in the InAlAs layer.

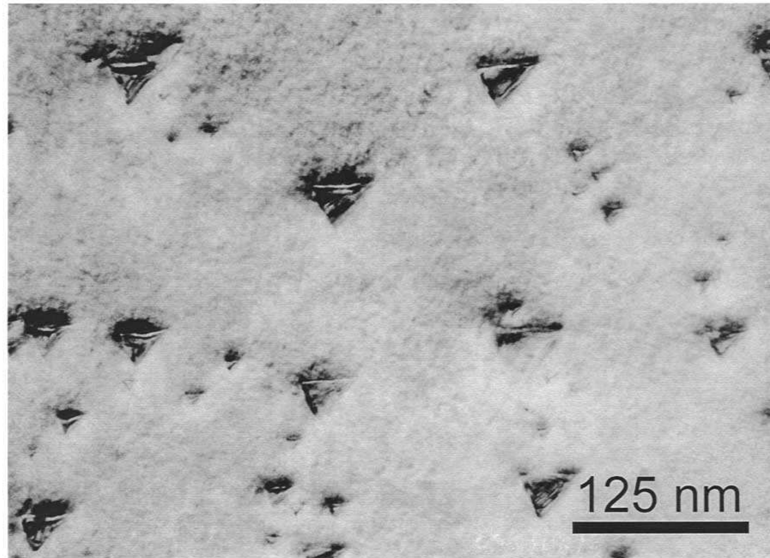

(a)

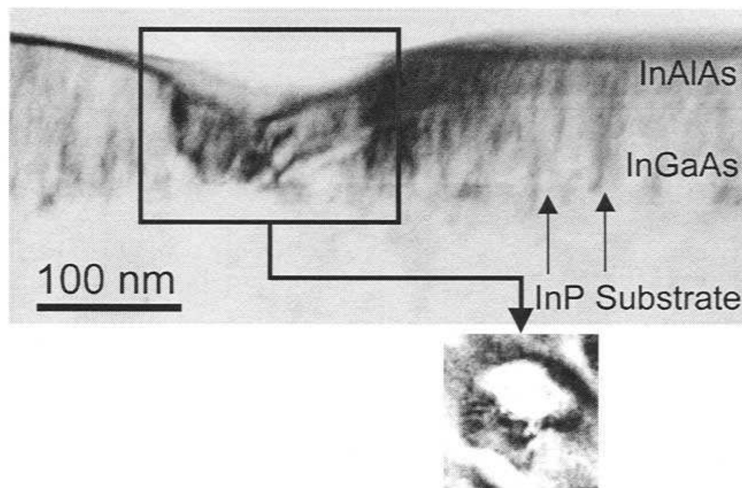

(b)

Fig. 6a) PVTEM micrograph of sample 695 (112)B. The triangle faceted defects are homogeneously distributed on the sample surface. **Figure 6b**. Cross-sectional TEM image of sample 695 (112) InP. The triangle defects have a faceted structure.